# Computational Design of Core/Shell Nanoparticles for Oxygen Reduction Reactions

Xu Zhang and Gang Lu*

Department of Physics and Astronomy, California State University Northridge, Northridge, California 91330-8268, United States

ABSTRACT: A computational strategy to design core/shell nanoparticle catalysts for oxygen reduction reactions (ORRs) is proposed based on multiscale modeling. Using a quantum mechanics/molecular mechanics (QM/MM) coupling method, we have studied the ORR on Pt−Cu core/shell nanoparticles with the size ranging from 3 to 8 nm. We have calculated the oxygen adsorption energy on the nanoparticle surface (a descriptor for ORR activity) as a function of the nanoparticle size and thickness of the Pt shell. We find that the Pt−Cu core/shell nanoparticles exhibit higher ORR activities than flat Pt(111) surfaces, consistent with experimental observations. We predict that the diameter of the core/shell nanoparticles should be larger than 7 nm to reach the peak of ORR activities. By examining the effects of ligand, quantum confinement, and surface strain, we confirm that the strain plays the dominant role on ORR activities for the core/shell nanoparticles. A universal relation between the surface strain and the oxygen adsorption energy is established based on which one can computationally screen and design core/shell nanoparticle catalysts for superior ORR activities.

$$E_O(\varepsilon) = a \times \varepsilon + b$$

SECTION: Surfaces, Interfaces, Porous Materials, and Catalysis
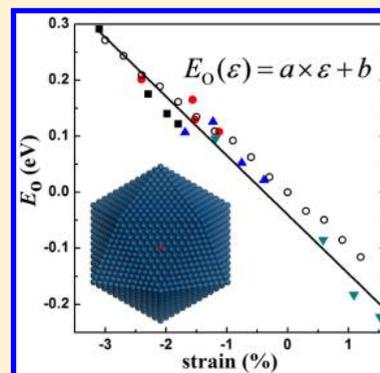
The oxygen reduction reaction (ORR) is a key chemical reaction in proton exchange membrane fuel cells (PEMFCs), which use hydrogen fuel and oxygen from the air to produce electricity, an attractive technology for generating clean and secure energy. However, the sluggish ORR kinetics at the cathode and the use of precious-metal-based catalysts pose two major roadblocks for broad deployment of PEMFCs. Tremendous effort has been devoted to the development of inexpensive, more stable, and highly efficient catalysts for ORRs.[1,2] Among them, Pt-based core/shell nanoparticles represent a particularly promising class of ORR catalysts.[3−12] On one hand, these core/shell particles exhibit superior ORR mass activities because Pt is eliminated from the core.[4−6] For example, Pt−Cu core/shell catalysts showed an increased mass activity of a factor of 4 over that of the commercial Pt catalysts.[6] On the other hand, the judicious selection of the core materials offers a means to achieve exceptional specific activities by optimizing the electronic and structural properties of the catalysts.[3,10−13] Recently, Strasser et al. demonstrated a novel concept that surface strain could be used to tune the catalytic activities of Pt-based core/shell nanoparticles, providing a general strategy to actively control the performance of the catalysts.[12] In particular, they found that the dealloyed Pt−Cu core/shell nanoparticles displayed uniquely high ORR reactivities owing to the surface strain. However, it is extremely challenging to measure accurately the surface strain on the Pt shell, which is crucial to elucidate the correlation between the strain and the enhanced ORR activities. In addition, there is no clear pathway as how to achieve the maximum ORR reactivity for a given combination of core/shell materials. More importantly, there is a lack of guidance in the search of an optimal combination of core/shell materials with superior ORR

activities. In this Letter, we propose a multiscale computational strategy to design core/shell nanoparticles for the ORR. We can determine the surface strain accurately from quantum mechanical (QM) calculations and establish a universal relation between the surface strain and the oxygen adsorption energy on the surface of the core/shell nanoparticles. Using the surface strain as a descriptor, we can then computationally screen core/shell particles for superior ORR activities.

QM simulations are often mandatory to deal with the creation and breaking of bonds in chemical reactions. However, such DFT simulations are computationally intensive, and as a result, they have not been used for core/shell particles larger than a few nanometers that are of practical interest. To overcome this difficulty, we have developed a multiscale quantum mechanics/molecular mechanics (QM/MM) approach that combines the accuracy of QM simulations with the efficiency of classical MM simulations.[14] More specifically, the DFT is applied to the reactive region for describing the chemical reaction accurately, while the long-range strain field of the nanoparticles is captured by the inexpensive MM calculations. The QM/MM method can reproduce the correct charge density surrounding the QM region, thus capturing the electronic effects such as quantum confinement, charge transfer, and polarization that are important in catalysis. As such, it is a valuable computational tool for designing nanoparticle catalysts that are otherwise beyond the reach of QM simulations. In this Letter, we first focus on Pt−Cu nanoparticles that have been

studied experimentally[6,12] and address some of the challenges encountered in the experiments. The Pt−Cu core/shell nanoparticles consist of Pt shell and Cu core, modeled by icosahedrons with twenty (111) facets, as shown in Figure 1.
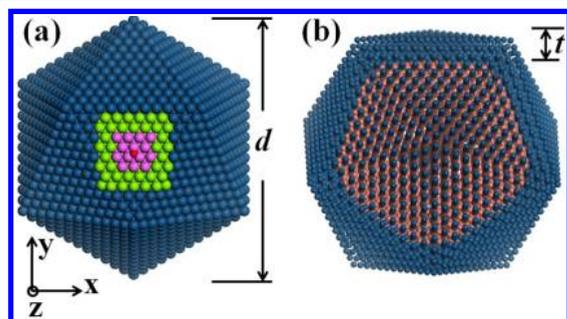
Figure 1. QM/MM models of the core/shell nanoparticles. (a) Partition of the entire system into the interior QM region (red and pink spheres), the boundary QM region (green spheres), and the MM region (blue spheres). The z direction is perpendicular to the (111) facet. The red sphere represents the adsorbed O atom, and d is the nanoparticle diameter. (b) The atomic structure of the Pt−Cu core/shell nanoparticle. Brown and blue spheres represent Cu and Pt atoms, respectively. t is the thickness of the Pt shell.

We consider four nanoparticles with d = 3.2, 4.8, 6.4, and 8.0 nm, corresponding to 923, 2869, 6525, and 12431 atoms, respectively. For each nanoparticle, three Pt shell thicknesses (t = 0.6, 0.8, and 1.0 nm) are examined, corresponding to three, four, and five Pt atomic layers, respectively. These are the same thicknesses as those reported in the experiment of Strasser et al.[12] We also include pure Pt nanoparticles in the calculations as the reference points. The ORR on the (111) facet of the nanoparticles is considered in both the present QM/MM simulations and the previous experiments.

It has been well-established that the oxygen surface adsorption energy E_O is a good descriptor of ORR activity in both pure metals and alloys.[15,16] If the binding between oxygen and a metal surface is too strong (i.e., E_O is more negative), the bottleneck of the ORR is the removal of adsorbed O and OH species. If the binding is too weak, the bottleneck is the dissociation of O_2 on the metal surface. It has been found that the flat Pt(111) surface binds 0.2 eV too strongly with oxygen.[16] Hence, the optimal or target value of E_O should be 0.2 eV higher than that on the flat Pt(111) surface. The goal of the study is to design core/shell particles so that E_O is less negative and as close as possible to the target value. There are three "knobs" that we can turn in the materials design, the size of nanoparticle (d), the thickness of Pt shell (t), and the choice of core material. According to Norskov et al.,[15] the effect of the water molecules on the oxygen adsorption is negligible; hence, we calculate E_O relative to the flat Pt(111) surface by placing an O atom at the fcc-hollow site on the (111) facet

$$E_O = (E_{QM/MM}[NP + O] - E_{QM/MM}[NP])$$
$$- (E_{QM}[Pt(111) + O] - E_{QM}[Pt(111)]) \quad (1)$$

where $E_{QM/MM}[NP + O]$ and $E_{QM/MM}[NP]$ are the total energies of the nanoparticles with and without the absorbed O atom calculated from the QM/MM method. $E_{QM}[Pt(111) + O]$ and $E_{QM}[Pt(111)]$ are the total energies of the flat Pt(111) surface with and without the absorbed O atom calculated from the conventional DFT method. The hcp-hollow site is

energetically unfavorable compared to the fcc-hollow site for O adsorption on the (111) facet of the nanoparticles. On the flat (111) surface, the QM/MM calculation yields the same E_O value as the stand-alone conventional DFT calculation, which validates the QM/MM method in terms of the energetics. The E_O values as a function of d and t for both core/shell and pure Pt nanoparticles are shown in Figure 2. We find that the pure
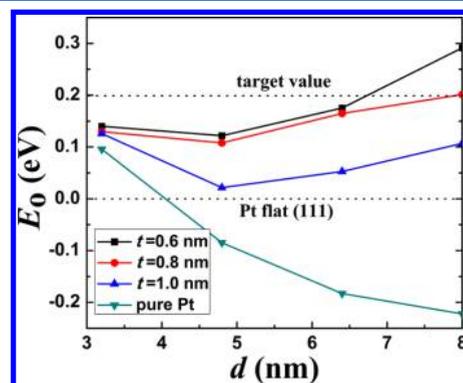
Figure 2. E_O on the (111) facet of the Pt−Cu core/shell and pure Pt nanoparticles. The horizontal lines indicate the E_O value for the flat Pt(111) surface and the target value for achieving the optimal ORR activity.

Pt nanoparticles cannot reach the target value of E_O for the reasonable particle sizes. The larger the particle size, the stronger the oxygen binding energy. When d is greater than 4 nm, the pure Pt nanoparticle has an even lower ORR activity than the flat Pt(111) surface. On the other hand, the Pt−Cu core/shell nanoparticles could offer higher ORR activities as both the black and red curves intersect the target line in Figure 2. These results are consistent with the experimental findings.[12] We also calculated E_O for two larger core/shell particles (d = 9.6 nm, t = 0.6 and 0.8 nm). The E_O value is 0.36 and 0.28 eV, respectively, well above the target value of 0.2 eV. Thus, the generic "volcano" behavior is indeed revealed for the Pt−Cu core/shell nanoparticles. It is observed that the thinner the Pt shell, the weaker the oxygen binding energy. We predict that the core/shell nanoparticle size has to be larger than 7 nm in order to reach the maximum ORR activities. This might explain why Strasser et al. did not observe the "volcano peak" in their experiments as their average particle size ranges from 3.4 to 5.1 nm, less than 7 nm.

There are three factors that may influence the oxygen adsorption energy E_O on the core/shell nanoparticles, including the ligand effect, quantum confinement, and strain. The ligand effect refers to the modification of the adsorptive properties by charge transfer between two dissimilar surface atoms in the vicinity of the adsorptive site.[17,18] In the Pt−Cu core/shell particles, the ligand effect could arise from the charge transfer between the core and shell atoms. To examine the possible ligand effect, we calculate E_O on a Pt thin film (three or four layers) with a Cu substrate and compare its energy to the pure Pt thin film without the Cu substrate. A slab model with seven atomic layers is used in the DFT calculations, and the positions of the atoms are determined based on the lattice constant of Pt to eliminate the strain effect. The conventional DFT calculations are performed on the slab model with the top two layers fully relaxed. The change in E_O is 0.03 and 0.005 eV for three and four Pt layers, respectively, much smaller than the typical energy variations (∼0.3 eV), as shown in Figure 2.

Therefore, in the context of the present work, the ligand effect is negligible.

Quantum confinement on the catalytic properties has been studied recently for Pt, Au, and other late transition metals.[19−21] Li et al. have calculated E_O on Pt nanoparticles with sizes ranging from 0.7 to 3.5 nm based on DFT.[19] They find that the quantum confinement effect in Pt particles vanishes for $d > 1.6$ nm as far as E_O in concerned. Because the particle sizes considered here exceed 3.2 nm, we do not expect the quantum confinement to be important. For the smallest particle $d = 3.2$ nm, we find that E_O is 0.1 eV higher than that of the flat surface, agreeing very well with that from the conventional DFT calculation as reported in Li et al.[19]

Because the surface strain is not uniformly distributed on the particle surface, we determine the local strain at the adsorption site as $\varepsilon = (1/N) \sum_{\langle i,j \rangle} ((r_{i,j} - r_0)/r_0)$. Here, i and j refer to the first- and second-nearest neighbors of the adsorption site on the surface. $\langle i,j \rangle$ indicates a pair of atoms with j being the nearest neighbor of i; N is the number of such pairs. $r_{i,j}$ and r_0 are the interatomic distances in the nanoparticle and the perfect bulk lattice, respectively. The strain ε as a function of d for the core/shell and pure Pt nanoparticles is displayed in Figure 3a. It is
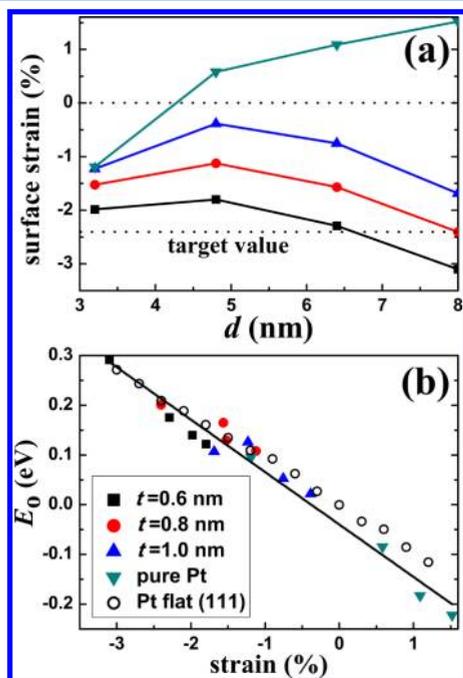
Figure 3. Surface strain on the core/shell nanoparticles. (a) Lateral strain on the (111) facet of the Pt−Cu core/shell and the pure Pt nanoparticles. The lower horizontal line indicates the target strain value for an optimal ORR activity. (b) Correlation between E_O and the surface strain for the nanoparticles and the Pt flat surface. There exists a universal linear relation between E_O and the strain.

found that all core/shell nanoparticles possess a compressive (or negative) strain, and the thinner the Pt shell, the greater the compressive strain. In contrast, the pure Pt nanoparticles exhibit a tensile strain for $d > 4$ nm. The tensile strain of 1.5% for the $d = 8$ nm nanoparticle agrees well with a previous result of 1.6% tensile strain on an icosahedral Pt nanoparticle.[22] The dependence of E_O versus ε for the core/shell nanoparticles is consistent with the d-band model.[23] For instance, a compressive strain of −2.4% in the nanoparticle with $d = 8$ nm and $t = 0.8$ nm leads to a downshift of the Pt d-band center

by 0.4 eV and weakening of O binding by 0.2 eV. On the other hand, a tensile strain of 1.5% in the pure Pt nanoparticle with $d = 8$ nm results in an upshift of the Pt d-band center by 0.2 eV and strengthening of O binding by 0.2 eV.

To examine the strain effect on ORR, we also calculate E_O as a function of ε on the flat Pt(111) surface. Remarkably, as shown in Figure 3b, there exists a universal linear relation between E_O and ε for both the core−shell and pure Pt nanoparticles as well as the flat Pt surface. Therefore, the surface strain plays a crucial role in determining ORR activities and may also be regarded as a descriptor for the ORR. The $E_O−\varepsilon$ relation in Figure 3b can be determined by a linear regression as

$$E_O(\varepsilon) = a \times \varepsilon + b \qquad (2)$$

where a is the slope, equal to −0.1 eV per 1% strain, and b represents the difference in E_O between the particles and the flat Pt surface at zero strain, equal to −0.04 eV.

Using the linear relation in eq 2, one can estimate E_O by determining the local surface strain at the active site using either inexpensive atomistic simulations based on empirical potentials or continuum finite-element calculations. This is possible because there is no forming or breaking of chemical bonds in the simulations of surface strain; thus, QM modeling is unnecessary. To demonstrate the computational strategy, we employ the empirical embedded atom method (EAM)[24] to estimate the surface strain of Pt−M core/shell nanoparticles with the core material M being either a pure metal or binary alloy. We then estimate E_O based on eq 2 to assess the ORR activity of these core−shell particles. All of the binary alloys considered here are thermodynamically stable and can be synthesized experimentally.[25−29]

Because tuning catalytic activity as a function of Pt shell thickness has been attempted before in experiments,[3] here we focus on tuning the ORR activity by varying the composition of core materials. We first examine elemental core materials with M = Pt, Fe, Co, Ni, Cu, Pd, Ag, and Au. For each core material, four different particle sizes are considered, as shown in different colored legends in Figure 4a; the Pt shell thickness is 0.6 nm, the same as that for all of the particles. The legends falling between the two dashed lines indicate that the corresponding
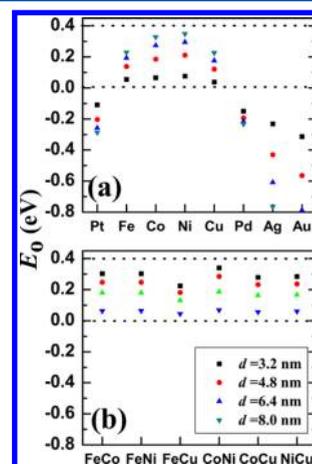
Figure 4. E_O of Pt−M core/shell nanoparticles with $t = 0.6$ nm. (a) M = Pt, Fe, Co, Ni, Cu, Pd, Ag, and Au; (b) M = FeCo, FeNi, FeCu, CoNi, CoCu, and NiCu. The nanoparticles falling between the two dashed lines have higher ORR activities than the flat Pt(111) surface.

core/shell particles have superior ORR activities compared to the flat Pt surface. Here, we determine the upper bound of E_O to be 0.4 eV based on the ORR volcano plots.[30] We predict that Fe, Co, Ni, and Cu can be used as the core materials to improve the ORR activity over the flat Pt(111) surface, whereas Ag and Au as the core materials would render inferior ORR activities. The E_O values from the EAM calculations are in good agreement with the QM/MM results for the pure Pt and Pt–Cu nanoparticles, validating the proposed computational strategy. The only exception is the smallest particle with d = 3.2 nm. In this case, the O adsorption site is very close to the icosahedral edge where the EAM potential does not reproduce well the DFT values. For Pt–Pd nanoparticles, E_O is insensitive to the particle size and slightly larger than the corresponding value of the pure Pt nanoparticle. This suggests that the Pt–Pd nanoparticles should exhibit a minor enhancement of ORR activity over Pt nanoparticles, consistent with the experimental observation.[31] On the basis of the results, we next intermix the four promising metals (Fe, Co, Ni, and Cu) to form random binary alloys with a 1:1 atomic ratio as the core materials, that is, M = FeCo, FeNi, FeCu, CoNi, CoCu, and NiCu. The results of the six binary alloys are shown in Figure 4b, and interestingly, all of these core/shell particles show superior ORR activities over the flat Pt surface. Therefore, these random binary alloys should also be considered as the core materials in the future development of core/shell particles. However, because Fe, Co, Ni, and Cu tend to be oxidized, it could be challenging to synthesize core/shell particles based these active metals. To circumvent this challenge, we also explore the binary alloys consisting of noble metals such as Ag and Pd as the core materials. Although Ag and Pd are not good candidates for the core materials by themselves, they may make good core materials by forming alloys. To test this hypothesis, we mix Fe, Co, Ni, and Cu with Ag or Pd to form random binary alloys (M = AgFe, AgCo, AgNi, AgCu, PdFe, PdCo, PdNi, and PdCu). In this case, we vary the atomic concentration of Ag and Pd in the random alloys from 20 to 50 atom %, and the results are summarized in Figure 5. It is found that for the same random
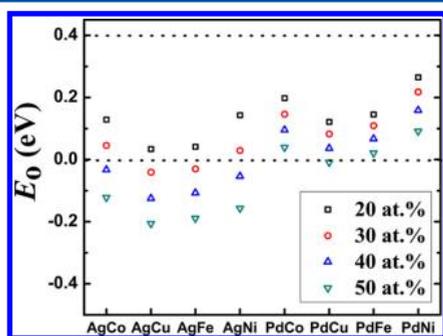
Figure 5. E_O of Pt–M core/shell nanoparticles with d = 8.0 nm and t = 0.6 nm. M = binary alloy: AgFe, AgCo, AgNi, AgCu, PdFe, PdCo, PdNi, and PdCu. The legend indicates the atomic content of the noble metal Ag or Pd.

alloy, the higher concentration of the noble metals, the stronger the oxygen binding energy. We predict that Fe–Pd, Co–Pd, and Ni–Pd are the promising candidates for the core materials. Although we have not considered ordered intermetallic alloys as the core materials in the present work, the same computational strategy can be applied to them as well.

Notwithstanding the enormous complexity of the ORR, we strive to provide a simple and clean picture here based on the strain effect so that a practical computational strategy can be formulated to aid the design of the core/shell particles. Although the surface strain plays a crucial role in controlling ORR activities in the core/shell particles, other factors such as shapes of the particles, active sites, and stabilities of the particles could also be important[10,11] but are not pursed in the present work. Despite these uncertainties, we still believe that the computational strategy could be used for a rapid screening of core/shell particles; on the basis of the results, one can then perform secondary screening by considering other factors.

In summary, we have proposed a multiscale computational strategy to design core/shell nanoparticles for the ORR. Using this approach, we study ORR on the Pt–Cu core/shell nanoparticles as a function of the particle size (3–8 nm) and the Pt shell thickness (0.6–1.0 nm). We find that the Pt–Cu core/shell nanoparticles have higher ORR activities than the flat Pt(111) surface, consistent with the experiments. We predict that the core/shell nanoparticles should be larger than 7 nm in diameter in order to achieve the maximum ORR activities. By examining the effects of the ligand, quantum confinement, and strain, we confirm that the ORR activity of the core/shell nanoparticles is primarily determined by the surface strain due to the lattice mismatch between the core/shell materials. A universal relation between the surface strain and the oxygen adsorption energy is established, which could serve as guidance for rapid screening of the core/shell particles. Finally, we demonstrate how one may start to design core/shell nanoparticles for superior ORR activities using the proposed computational strategy.

■ COMPUTATIONAL DETAILS

QM/MM Method. In the QM/MM approach, the entire system is partitioned into two spatial domains, a QM region treated by the constrained DFT[32−34] and a MM region treated by empirical atomistic simulations. The QM region is further divided into an interior QM region and a boundary QM region. The former involves bond breaking, chemical reaction, charge transfer, and so forth. The latter serves as a buffer region where there is no significant perturbation to the charge density. The MM atoms interact directly with the boundary QM atoms but only indirectly with the interior QM atoms. The total energy of the QM/MM system can be expressed as

$$E_{tot} = E^{DFT}[\rho_{QM}; \mathbf{R}_{QM}] + E^{MM}[\mathbf{R}_{QM}^b \cup \mathbf{R}_{MM}]$$
$$- E^{MM}[\mathbf{R}_{QM}^b] \tag{3}$$

where the first term denotes the energy of the entire QM region calculated via the constrained DFT. The last two terms are the energy of the combined QM boundary/MM region and the QM boundary region, respectively, as determined by the empirical MM simulations. $\mathbf{R}_{QM}$, $\mathbf{R}_{QM}^b$, and $\mathbf{R}_{MM}$ represent atomic coordinates in the entire QM, the QM boundary, and the MM regions, respectively. ρ_{QM} indicates the QM charge density. As a key component of the QM/MM method, the constrained DFT allows a self-consistent determination of ρ_{QM} by constraining it to a predetermined charge density in the boundary region. The essence of the QM/MM method is to ensure that the QM region is treated in the presence of appropriate boundary conditions provided by the charge density and potentials of the MM atoms. The technical details

and validations of the QM/MM method can be found elsewhere.[14]

Computational Parameters. As shown in Figure 1, the QM region measures 17 Å × 17 Å × 8 Å in *x*, *y*, and *z* directions, respectively, where the innermost 8.4 Å × 7.3 Å × 4 Å is the interior QM region containing the reactive site for oxygen adsorption. There are 140, 167, 187, and 193 QM atoms for the four nanoparticle sizes, respectively. The MM region consists of the rest of the system where the strain effect due to the lattice mismatch between the core and shell is captured. The DFT calculations are performed using the VASP package[35,36] with the projector augmented wave pseudopotentials[37] and Perdew–Burke–Ernzerhof generalized gradient approximation (PBE-GGA).[38] The energy cutoff is 400 eV. The EAM potentials[39] are used in the MM simulations, which have been rescaled to yield the same lattice constant and bulk modulus as those from DFT. The atomic relaxation is carried out with the conjugate gradient algorithm, and the force convergence criterion is 0.02 eV/Å. For calculations of O adsorption on a flat Pt(111) surface with or without strain, we use the standard DFT with a (4 × 2) four-layer slab with the top two layers fully relaxed. The k-point mesh of 4 × 5 × 1 in the surface Brillouin zone is used.

■ AUTHOR INFORMATION

Corresponding Author
*E-mail: ganglu@csun.edu.

Notes
The authors declare no competing financial interest.

■ ACKNOWLEDGMENTS

■ REFERENCES

(1) Gasteiger, H. A.; Markovic, N. M. Just a Dream - or Future Reality? *Science* **2009**, *324*, 48–49.

(2) Debe, M. K. Electrocatalyst Approaches and Challenges for Automotive Fuel Cells. *Nature* **2012**, *486*, 43–51.

(3) Wang, J. X.; Inada, H.; Wu, L.; Zhu, Y.; Choi, Y. M.; Liu, P.; Zhou, W. P.; Adzic, R. R. Oxygen Reduction on Well-Defined Core–Shell Nanocatalysts: Particle Size, Facet, and Pt Shell Thickness Effects. *J. Am. Chem. Soc.* **2009**, *131*, 17298–17302.

(4) Adzic, R. R.; Zhang, J.; Sasaki, K.; Vukmirovic, M. B.; Shao, M.; Wang, J. X.; Nilekar, A. U.; Mavrikakis, M.; Valerio, J. A.; Uribe, F. Platinum Monolayer Fuel Cell Electrocatalysts. *Top. Catal.* **2007**, *46*, 249–262.

(5) Wang, D.; Xin, H. L.; Hovden, R.; Wang, H.; Yu, Y.; Muller, D. A.; DiSalvo, F. J.; Abruna, H. D. Structurally Ordered Intermetallic Platinum–Cobalt Core–Shell Nanoparticles with Enhanced Activity and Stability as Oxygen Reduction Electrocatalysts. *Nat. Mater.* **2013**, *12*, 81–87.

(6) Mani, P.; Srivastava, R.; Strasser, P. Dealloyed Pt–Cu Core–Shell Nanoparticle Electrocatalysts for Use in PEM Fuel Cell Cathodes. *J. Phys. Chem. C* **2008**, *112*, 2770–2778.

(7) Mazumder, V.; Chi, M.; More, K. L.; Sun, S. Core/Shell Pd/FePt Nanoparticles as an Active and Durable Catalyst for the Oxygen Reduction Reaction. *J. Am. Chem. Soc.* **2010**, *132*, 7848–7849.

(8) Guo, S.; Zhang, S.; Su, D.; Sun, S. Seed-Mediated Synthesis of Core/Shell FePtM/FePt (M = Pd, Au) Nanowires and Their Electrocatalysis for Oxygen Reduction Reaction. *J. Am. Chem. Soc.* **2013**, *135*, 13879–13884.

(9) Neyerlin, K. C.; Srivastava, R.; Yu, C. F.; Strasser, P. Electrochemical Activity and Stability of Dealloyed Pt–Cu and Pt–Cu–Co Electrocatalysts for the Oxygen Reduction Reaction (ORR). *J. Power Sources* **2009**, *186*, 261–267.

(10) Guo, S.; Zhang, S.; Sun, S. Tuning Nanoparticle Catalysis for Oxygen Reduction Reaction. *Angew. Chem., Int. Ed.* **2013**, *52*, 2–21.

(11) Oezaslan, M.; Hasche, F.; Strasser, P. Pt-Based Core–Shell Catalyst Architectures for Oxygen Fuel Cell Electrodes. *J. Phys. Chem. Lett.* **2013**, *4*, 3273–3291.

(12) Strasser, P.; Koh, S.; Anniyev, T.; Greeley, J.; More, K.; Yu, C.; Liu, Z.; Kaya, S.; Nordlund, D.; Ogasawara, H.; Toney, M. F.; Nilsson, A. Lattice-Strain Control of the Activity in Dealloyed Core–Shell Fuel Cell Catalysts. *Nat. Chem.* **2010**, *2*, 454–460.

(13) Zhang, L.; Iyyamperumal, R.; Yancey, D. F.; Crooks, R. M.; Henkelman, G. Design of Pt-Shell Nanoparticles with Alloy Cores for the Oxygen Reduction Reaction. *ACS Nano* **2013**, *7*, 9168–9172.

(14) Zhang, X.; Lu, G.; Curtin, W. A. Multiscale Quantum/Atomistic Coupling Using Constrained Density Functional Theory. *Phys. Rev. B* **2013**, *87*, 054113.

(15) Norskov, J. K.; Rossmeisl, J.; Logadottir, A.; Lindqvist, L.; Kitchin, J. R.; Bligaard, T.; Jonsson, H. Origin of the Overpotential for Oxygen Reduction at a Fuel-Cell Cathode. *J. Phys. Chem. B* **2004**, *108*, 17886–17892.

(16) Stamenkovic, V. R.; Mun, B. S.; Mayrhofer, K. J. J.; Ross, P. N.; Markovic, N. M.; Rossmeisl, J.; Greeley, J.; Norskov, J. K. Changing the Activity of Electrocatalysts for Oxygen Reduction by Tuning the Surface Electronic Structure. *Angew. Chem., Int. Ed.* **2006**, *45*, 2897–2901.

(17) Rodriguez, J. A.; Goodman, D. W. The Nature of the Metal–Metal Bond in Bimetallic Surfaces. *Science* **1992**, *257*, 897–903.

(18) Stamenkovic, V. R.; Fowler, B.; Mun, B. S.; Wang, G.; Ross, P. N.; Lucas, C. A.; Markovic, N. M. Improved Oxygen Reduction Activity on Pt3Ni(111) via Increased Surface Site Availability. *Science* **2007**, *315*, 493–497.

(19) Li, L.; Larsen, A. H.; Romero, N. A.; Morozov, V. A.; Glinsvad, C.; Abild-Pedersen, F.; Greeley, J.; Jacobsen, K. W.; Norskov, J. K. Investigation of Catalytic Finite-Size-Effects of Platinum Metal Clusters. *J. Phys. Chem. Lett.* **2013**, *4*, 222–226.

(20) Peterson, A. A.; Grabow, L. C.; Brennan, T. P.; Shong, B.; Ooi, C.; Wu, D. M.; Li, C. W.; Kushwaha, A.; Medford, A. J.; Mbuga, F.; Li, L.; Norskov, J. K. Finite-Size Effects in O and CO Adsorption for the Late Transition Metals. *Top. Catal.* **2012**, *55*, 1276–1282.

(21) Kleis, J.; Greeley, J.; Romero, N. A.; Morozov, V. A.; Falsig, H.; Larsen, A. H.; Lu, J.; Mortensen, J. J.; Dulak, M.; Thygesen, K. S.; Norskov, J. K.; Jacobsen, K. W. Finite Size Effects in Chemical Bonding: From Small Clusters to Solids. *Catal. Lett.* **2011**, *141*, 1067–1071.

(22) Wu, J.; Qi, L.; You, H.; Gross, A.; Li, J.; Yang, H. Icosahedral Platinum Alloy Nanocrystals with Enhanced Electrocatalytic Activities. *J. Am. Chem. Soc.* **2012**, *134*, 11880–11883.

(23) Mavrikakis, M.; Hammer, B.; Norskov, J. K. Effect of Strain on the Reactivity of Metal Surfaces. *Phys. Rev. Lett.* **1998**, *81*, 2819–2822.

(24) Daw, M. S.; Baskes, M. I. Embedded-Atom Method: Derivation and Application to Impurities, Surfaces, and Other Defects in Metals. *Phys. Rev. B* **1984**, *29*, 6443–6453.

(25) Li, X.; Shao, H.; Liu, T. Synthesis of Nanoparticles and Their Properties by Hydrogen Plasma Metal Reaction. In *Trends in Nanotechnology Research*; Eugene, V. D., Ed.; Nova Science Publishers, New York, 2004; pp 99–132.

(26) Teranishi, T.; Miyake, M. Novel Synthesis of Monodispersed Pd/Ni Nanoparticles. *Chem. Mater.* **1999**, *11*, 3414–3416.

(27) Zhang, Z.; Nenoff, T. M.; Leung, K.; Ferreira, S. R.; Huang, J. Y.; Berry, D. T.; Provencio, P. P.; Stumpf, R. Room-Temperature Synthesis of Ag–Ni and Pd–Ni Alloy Nanoparticles. *J. Phys. Chem. C* **2010**, *114*, 14309–14318.

(28) Damle, C.; Biswas, K.; Sastry, M. Synthesis of Nanoscale Fe–Ag Alloy within Thermally Evaporated Fatty Acid Films. *Nanotechnology* **2002**, *13*, 103.

(29) Tsuji, M.; Hikino, S.; Tanabe, R.; Matsunaga, M.; Sano, Y. Syntheses of Ag/Cu Alloy and Ag/Cu Alloy Core Cu Shell Nanoparticlesusing a Polyol Method. *CrystEngComm* **2010**, *12*, 3900−3908.

(30) Greeley, J.; Stephens, I. E. L.; Bondarenko, A. S.; Johansson, T. P.; Hansen, H. A.; Jaramillo, T. F.; Rossmeisl, J.; Chorkendorff, I.; Norskov, J. K. Alloys of Platinum and Early Transition Metals as Oxygen Reduction Electrocatalysts. *Nat. Chem.* **2009**, *1*, 552−556.

(31) Zhang, J.; Mo, Y.; Vukmirovic, M. B.; Klie, R.; Sasaki, K.; Adzic, R. R. Platinum Monolayer Electrocatalysts for O_2 Reduction: Pt Monolayer on Pd(111) and on Carbon-Supported Pd Nanoparticles. *J. Phys. Chem. B* **2004**, *108*, 10955−10964.

(32) Zhao, Q.; Parr, R. G. Constrained-Search Method to Determine Electronic Wave Functions from Electronic Densities. *J. Chem. Phys.* **1992**, *98*, 543−548.

(33) Zhao, Q.; Morrison, R. C.; Parr, R. G. From Electron Densities to Kohn−Sham Kinetic Energies, Orbital Energies, Exchange−Correlation Potentials, and Exchange−Correlation Energies. *Phys. Rev. A* **1994**, *50*, 2138−2142.

(34) Wu, Q.; Van Voorhis, T. Direct Optimization Method to Study Constrained Systems within Density-Functional Theory. *Phys. Rev. A* **2005**, *72*, 024502.

(35) Kresse, G.; Hafner, J. Ab Initio Molecular Dynamics for Liquid Metals. *Phys. Rev. B* **1993**, *47*, 558−561.

(36) Kresse, G.; Furthmuller, J. Efficient Iterative Schemes for Ab Initio Total-Energy Calculations Using a Plane-Wave Basis Set. *Phys. Rev. B* **1996**, *54*, 11169−11186.

(37) Blochl, P. E. Projector Augmented-Wave Method. *Phys. Rev. B* **1994**, *50*, 17953−17979.

(38) Perdew, J. P.; Burke, K.; Ernzerhof, M. Generalized Gradient Approximation Made Simple. *Phys. Rev. Lett.* **1996**, *77*, 3865−3868.

(39) Zhou, X. W.; Johnson, R. A.; Wadley, H. N. G. Misfit-Energy-Increasing Dislocations in Vapor-Deposited CoFe/NiFe Multilayers. *Phys. Rev. B* **2004**, *69*, 144113.